NMR and Computational Evidence That High-Affinity Bradykinin Receptor Antagonists Adopt C-Terminal β-Turns

Donald J. Kyle,*,† Paul R. Blake,‡ Damon Smithwick,‡ Lora M. Green,‡ Jennifer A. Martin,† Jacqueline A. Sinsko,† and Michael F. Summers‡

Scios Nova Inc., 6200 Freeport Centre, Baltimore, Maryland 21224, and Department of Chemistry and Biochemistry, University of Maryland Baltimore County, Baltimore, Maryland 21228

Received December 28, 1992

Three tetrapeptides were prepared, each corresponding to the four C-terminal amino acid residues of highly potent, second-generation bradykinin receptor antagonists. The tetrapeptides are (IA) Ser-D-Phe-Oic-Arg, (IIA) Ser-D-Tic-Oic-Arg, and (IIIA) Ser-D-Hype(*trans*-propyl)-Oic-Arg. Solution conformations for each were determined by incorporating interproton distance restraints, determined by 2D NMR experiments performed in water at neutral pH, into a series of distance geometry/simulated annealing model building calculations. Similarly, systematic conformational analyses were performed for each using molecular mechanics calculations. Both the NMR-derived structures, as well as the calculated structures, are shown to adopt a β-turn as the primary conformation. Excellent agreement between the predicted structures and the NMR-derived structures is demonstrated. Aside from being the first examples of linear tetrapeptides reported to be ordered in aqueous solvent, the results presented support the hypothesis that high-affinity bradykinin receptor antagonists must adopt C-terminal β-turn conformations.

Introduction

Bradykinin is a linear nonapeptide hormone (Arg^1-Pro^2-Pro^3-Gly^4-Phe^5-Ser^6-Pro^7-Phe^8-Arg^9) generated as a result of the activity of kallikreins, a group of proteolytic enzymes present in most tissues and body fluids, on kininogen. Once released, bradykinin elicits many pathophysiological responses including pain and hyperalgesia by stimulating C- and A-fibers in the periphery.[1-7] There is also considerable evidence that bradykinin contributes to the inflammatory response, sepsis, airway disorders including asthma, and symptoms associated with rhinoviral infection.[8-13] These dramatic activities of bradykinin have been intensely studied for several decades with the long-term vision of developing potential therapeutic agents which could act as competitive antagonists at the bradykinin receptor.

The ultimate preparation of novel nonpeptide bradykinin receptor antagonists is a formidable challenge. The severity of the problem is enhanced significantly due to the lack of either X-ray crystallographic or NMR data pertaining to the receptor–ligand complex. Moreover, there has never been a report describing any nonpeptide antagonists that are potent, selective, and competitive for the bradykinin receptor, thereby eliminating the typical formulation of a structure–activity relationship. In the absence of this type of information, the approach of preparing conformationally constrained peptide analogues of the native ligand represents prudent methodology. This approach has led to the recent discovery of two new classes of second-generation peptide bradykinin antagonists with very high affinities for the B2 receptor.[14-17]

Both classes are of the general sequence D-Arg^0-Arg^1-Pro^2-W^3-Gly^4-X^5-Ser^6-Y^7-Z^8-Arg^9, where W is either proline or hydroxyproline and X is an aromatic side chain-containing amino acid such as phenylalanine or thienylalanine (Thi). Historically, it has been shown that position 7, "Y", must be held by a D aromatic amino acid in order to obtain a competitive antagonist.[18] One of the two new classes fits into that profile since its members contain either the conformationally constrained phenylalanine residue, D-Tic (tetrahydroisoquinolinecarboxylic acid), or D-Phe itself at position 7. The other class represents a break from this historical requirement in that among its members are alkyl ethers of D-4-hydroxyproline at position 7. For both classes, however, position 8, "Z", is held by another conformationally constrained amino acid, usually L-Tic or L-Oic (octahydroindolecarboxylic acid). Representative amino acid sequences from each of these classes as well as their in vitro pharmacology are shown in Table I.

On the basis of empirical energy calculations and systematic conformational searches performed on model peptides, it has been suggested that the high receptor affinities of some of these new constrained peptides is related to their high propensities for adopting C-terminal β-turn conformations.[15,16] We recently reported in a communication that a linear tetrapeptide corresponding to the C-terminal four residues in one of the new class of antagonists adopts a β-turn in aqueous solution.[19] Here we extend the computational and spectroscopic detail with respect to that specific compound and include for the first time similar structural analyses for model tetrapeptides corresponding to the other classes of highly potent second-generation bradykinin receptor antagonists.

Methods

NMR and computational studies were performed on tetrapeptides IA, IIA, and IIIA (Table II) and IB, IIB, and IIIB (Table III), respectively, to determine if these linear tetrapeptides are capable of adopting β-turns. These peptides serve as representatives of the C-terminal portion of the two generations of known bradykinin antagonists.

1. **Computational Methodology.** Systematic conformational searches were performed on model compounds representing the four tetrapeptides described in Table II. These models are structurally depicted in Table III. Unlike peptide IIIA, no conformational analysis describing the C-terminal end of peptides

† Scios Nova Inc.
‡ University of Maryland Baltimore County.

0022-2623/93/1836-1450$04.00/0

Table I. Primary Amino Acid Sequences and in Vitro Pharmacology for Three Representative Second-Generation Bradykinin B2 Receptor Antagonists

peptide number	amino acid sequence	K_i (nM) guinea pig ileum[a]	pA_2 guinea pig ileum
I	D-Arg^0-Arg^1-Pro^2-Pro^3-Gly^4-Phe^5-Ser^6-D-Phe^7-Oic^8-Arg^9	0.75 ± 0.02	8.3 ± 0.07
II	D-Arg^0-Arg^1-Pro^2-Hyp^3-Gly^4-Thi^5-Ser^6-D-Tic^7-Oic^8-Arg^9	0.11 ± 0.04	8.7 ± 0.06
III	D-Arg^0-Arg^1-Pro^2-Hyp^3-Gly^4-Thi^5-Ser^6-D-Hype(*trans*-propyl)^7-Oic^8-Arg^9	0.16 ± 0.04	8.5 ± 0.02

[a] K_i values and pA_2 data were determined using standard methods previously reported.[39]

Table II. Tetrapeptide Model Compounds Representing the C-Terminal Portion of Representative Second-Generation Bradykinin B2 Receptor Antagonists

peptide	amino acid sequence
IA	H-Ser-D-Phe-Oic-Arg-OH
IIA	H-Ser-D-Tic-Oic-Arg-OH
IIIA	H-Ser-D-Hype(*trans*-propyl)-Oic-Arg-OH

Table III. Model Structures Used in the Conformational Analysis Experiments

model peptide	structure
IB	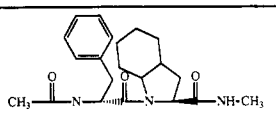
IIB	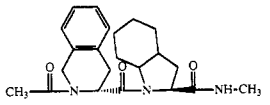
IIIB	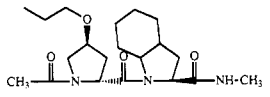

IA or IIA has been reported. To complete the series, an analysis similar to that reported for peptide IIIA was performed as follows.

All energy calculations were carried out using the program CHARMm,[20] version 21, on a Silicon Graphics 4D120GTXB workstation. In each case all amide bonds were assumed to exist in the trans geometry in conformity with the observations made in previous NMR experiments.[21,22] With the exception of model IB, the dihedral angles corresponding to ϕ_1, ϕ_2 (where ϕ_i corresponds to the backbone dihedral angle for residue i defined by the four adjacent amino acid backbone atoms C_{i-1}–N_i–$C\alpha_i$–C_i) in each model peptide are incorporated into either a five- or six-membered ring, thereby limiting their rotational degrees of freedom. Hence, a 10° grid search was performed on those dihedral angles corresponding to ψ_1 and ψ_2 (where ψ_i corresponds to the backbone dihedral angle for residue i defined by the four adjacent amino acid backbone atoms N_i–$C\alpha_i$–C_i–N_{i+1}) which dominate the overall backbone conformational states. At each grid point the ψ_1, ψ_2 dihedral angles were constrained to the specific grid value and 500 steps of Adopted-Basis-Newton-Raphson energy minimization were performed. Since the backbone dihedral angle ϕ in D-Phe is not inherently constrained as is the case for both D-Tic and the *trans*-propyl ether of D-4-hydroxyproline (D-Hype(*trans*-propyl)), the ψ_1, ψ_2 10° grid search was performed on IB while holding ϕ_1 fixed at 54°. That this is a highly favored value for this particular dihedral angle is clear on the basis of the classical Ramachandran plot for any D-amino acid wherein the favorable ϕ,ψ angles corresponding to an L-amino acid are inverted. In peptide IIB, which contains a tetrahydroisoquinolinecarboxylic acid (Tic) residue, both endo and exo boat forms of the saturated ring were considered explicitly. Moreover, each conformational search was performed with and without the contribution from the Coulombic potential in the overall potential energy expression. In each instance, the structural results obtained were the same, thus suggesting that the observed conformational preferences were driven by forces other than poorly represented atomic charges. Throughout this report the data presented have been taken from the simulations in which the complete CHARMm force field (including the electrostatic term) was used.

Table IV. Experimentally Determined Analytical Data for Peptides IA, IIA, and IIIA

peptide	fast atom bombardment MS $[M+H]_{calc}$	fast atom bombardment MS $[M+H]_{obs}$	amino acid analysis Ser	amino acid analysis Phe	amino acid analysis Arg	analytical HPLC,[a] R_t (min)
IA	572.59	572.59	1.00		1.21	19
IIA	560.51	560.51	1.00	0.92	1.10	15
IIIA	568.09	568.09	1.00		0.83	18

[a] HPLC performed using a C_{18} Vydac, 250 mm × 4.6 mm, 300-Å resin. Solvent gradient was from 5% to 40% acetonitrile in water, at a flow rate of 1.0 mL min^{-1}. UV detection was done at 220 nM.

2. Synthesis. The three linear tetrapeptides shown in Table II were synthesized by the solid-phase method of Merrifield[23] using standard procedures on a MilliGen Biosearch 9600 peptide synthesizer. Protected (*tert*-butyloxycarbonyl) amino acids were purchased from Bachem Bioscience (Philadelphia, PA) with the exception of the Boc-protected *trans*-propyl ether of D-4-hydroxyproline (Boc-D-Hype(*trans*-propyl)), whose preparation has been described elsewhere,[19] and Oic which was prepared by the literature method.[24] Boc-protected amino acid PAM (phenylacetamidomethyl) resins were purchased from Applied Biosystems (Foster City, CA). Single diisopropylcarbodiimide-mediated coupling reactions were run on the automatic synthesizer with the first amino acid routinely recoupled to the resin. Peptides were liberated from the resin by anhydrous liquid HF (10 mL/g of resin) containing 10% anisole at 0 °C for 1 h. All peptides were purified by RPHPLC on a Vydac C_{18} column using an CH_3CN/H_2O (0.1% TFA) gradient. All peptides were characterized by analytical HPLC, amino acid analysis, and FABMS, the results of which are summarized in Table IV.

3A. NMR Data Collection and Processing. NMR studies were carried out on the three tetrapeptides listed in Table II. To ensure that the structural tendencies of these peptides were not influenced by ordering solvents (e.g., dioxane), all NMR studies were carried out exclusively in aqueous solution.

Two-dimensional NMR data were obtained for all peptides in either 90% H_2O/10% D_2O or D_2O, T = 37.5 °C, and pH* values in the range 4.4–4.8. Amide-exchange studies were carried out with the solution pH values adjusted to ca. 7.6. NMR data were obtained with GE GN-500 (500.1 MHz, ^1H) and Omega-PSG 600 (599.7 MHz, ^1H) NMR spectrometers. 2-Dimensional (2D) homonuclear data were collected at 500 MHz with a spectral width of 7692.3 Hz in the acquisition dimension (3.76 Hz/point) and 256 complex states[25] blocks in the t_1 dimension. Suppression of the H_2O resonance was achieved using a 2-s Dante pulse train[26] consisting of 5° pulses separated by 100 μs. To allow for dipolar relaxation of proton resonances residing close to water, a SCUBA sequence[27] was inserted prior to the first pulse of the 2D sequence. For HOHAHA data, a $90^{\phi+1}$–homospoil–$90^{\phi-1}$ pulse train[28] was inserted prior to acquisition to aid in suppression of the dispersive base line due to residual H_2O which had relaxed during the t_1 delay and 8.8-kHz spin lock period. Data were transferred via ethernet to Silicon Graphics computers for processing using either FTNMR or FELIX. All data were processed with a 3-Hz Gaussian broadening function in t_2 and a 70°-shifted sine squared window function in t_1. The double quantum filtered COSY data were processed with an additional 90°-shifted sine squared filter in the t_1 dimension.

3B. NMR Signal Assignments. Proton spin systems were identified on the basis of scalar coupling networks defined by (2D) homonuclear Hartmann Hahn (HOHAHA) data.[29,30] For specific assignments of the side chain protons of Oic, ^1H-correlated spectroscopy[31] (COSY) data alone was insufficient due to spectral crowding and overlap in the upfield region of the spectrum. As such, the collection of heteronuclear multiple quantum corre-

lated[32] (HMQC) spectra was employed to make complete and unambiguous assignments for this side chain. 2D nuclear Overhauser effect[33,34] (NOESY) data were subsequently employed to identify through space proton–proton distances for the use in distance geometry (DG)-based structure calculations.

4. NMR-Based Structure Calculations. Structural modeling was performed with the DSPACE software package on Silicon Graphics computers. Templates that define the primary distance restraints were generated using idealized covalent bond distances and bond angles. Distance geometry/simulated annealing (DG/SA) models were generated with primary restraints only in order to establish that the models were sufficiently flexible in the absence of NOE restraints.[35] Structures were generated subsequently with the addition of "loose" distance restraints that represent the experimentally-observed nuclear Overhauser effect (NOE) data. Thus, distance restraints of 1.8–2.7, 1.8–3.3, and 1.8–4.5 Å were employed to represent qualitatively observed strong, medium, and weak NOE cross-peak intensities, respectively. Rotating frame Overhauser effect[36] (ROE) data were collected to enable differentiation of cross peaks resulting from direct NOE and spin diffusion effects.

For each peptide, 30 independent DG structures were generated by performing 10-Å randomizations of all atomic coordinates, followed by sequential steps of simulated annealing and conjugate gradient minimization (SA/CGM).[37,38] The lowest penalty value obtained from these calculations was used to generate a minimum penalty target (value increased by ca. 60%) for subsequent variable velocity structure refinement calculations. Final structures were generated from random initial coordinates using cycles of SA/CGM in an automated manner. An average of three passes through the DG/SA routine were necessary to achieve the low-penalty target. A total of 60 structures were generated in this manner for each tetrapeptide, 30 of which were generated with inclusion of NOE-derived distance restraints and 30 generated with primary distance restraints only.

5. In Vitro Assays. Bradykinin B2 receptor affinities were determined by K_i and pA_2 values measured in guinea pig ileal membrane or tissue preparations respectively using methods previously reported.[39] These data are presented in Table I. Guinea pig ileum is known to express only B2 bradykinin receptors.[40] At concentrations up to 10 μM, none of the peptides showed any agonist activity on the tissues and were competitive antagonists. Cumulative dose–response curves were constructed to bradykinin in the absence and in the presence of increasing concentrations of bradykinin antagonists (0.1–10.0 μM).

Results and Discussion

1A. Computational Analysis of Model Compounds. Potential energy contour plots describing the lowest 5 kcal mol^{-1} of the overall potential energy surface for each of the three model peptides are shown in Figure 1. The contour interval is 0.5 kcal mol^{-1}. Inspection of each plot leads to the conclusion that each pair of unnatural amino acids, D-Tic-Oic, D-Phe-Oic, D-Hype(*trans*-propyl)-Oic impose severe conformational restriction. In particular, the angle ψ_1 is restricted to values within the range of −180° to −120°, for each of the three model systems. One exception is for model IIB wherein a second range of ψ_1 (−90° to −50°) is allowed due to the presence of another local energy minimum which is 1.5 kcal mol^{-1} higher in energy than the global energy minimum. The dihedral angle ψ_2 ranges in each model from +90.0° to −90.0°, although there are only two local energy minima centered approximately at ψ_2 = +45° and ψ_2 = −45°. For model IIB, the additional potential energy well corresponds to a ψ_2 value of +45.0°.

1B. Analysis of Model IB. There is a single, broad potential energy well apparent in the lowest 5 kcal mol^{-1} of the overall potential energy surface obtained from a 10° grid scan about the dihedral angles ψ_1 and ψ_2 in model IB. The deepest portion of this well is centered about ψ_1 = −150°, ψ_2 = −40.0° and has an energy value of 2.5 kcal mol^{-1}. The ϕ, ψ values and corresponding potential energy

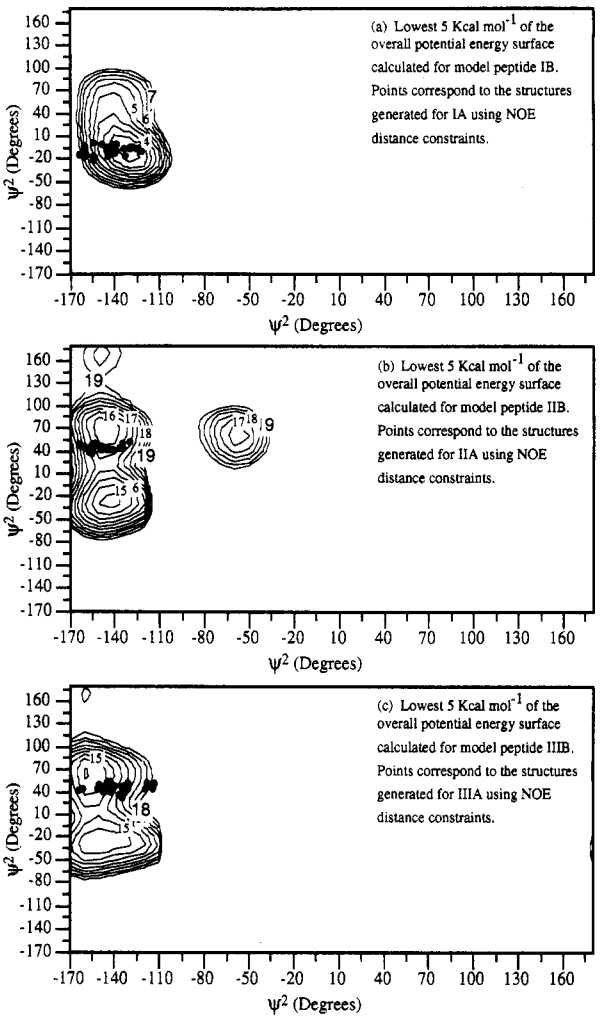

Figure 1. Lowest 5 kcal mol^{-1} of the calculated overall potential energy surface for (a) model IB, (b) model IIB, and (c) model IIIB. The contour interval is 0.5 kcal mol^{-1}, and for each the highest (outermost) and lowest contour energy values are labeled. Superimposed on the contour plots are values for ψ_{i+1} and ψ_{i+2} from each of the 30 structures generated from the NMR data for (a) peptide IA, (b) peptide IIA, and (c) peptide IIIA.

for a representative conformation extracted from the well is presented in Table V. This single potential energy well is centered about ψ_1, ψ_2 values corresponding to β-turn conformations. For this particular model, the β-turn conformation appears highly favored above all others with only slight fluctuation in the carbonyl oxygen (residue i) to amide proton (residue i + 3) hydrogen bond angle. A representative conformation extracted from this local energy minimum is shown in Figure 2a.

1C. Analysis of Model IIB. There are three local energy minima of approximately equivalent area in the lowest 5 kcal mol^{-1} of the overall potential energy surface obtained from a 10° grid scan of the dihedral angles, ψ_1, ψ_2 in model IIB. The deepest well is centered about ψ_1 = −150.0°, ψ_2 = −40.0° and has a lowest energy contour of 19.5 kcal mol^{-1}. Related to this well is a second which differs in potential energy from the first by 0.5 kcal mol^{-1} and is centered about ψ_1 = −150°, ψ_2 = +45.0. The barrier between the two conformations is approximately 1.0 kcal mol^{-1}. Representative conformations extracted from each of these energy wells correspond to β-turn-like structures. Finally, a third potential energy well, separated from the other two by a barrier greater than 5 kcal mol^{-1}, is centered about ψ_1 = −60.0°, ψ_2 = +60.0°. The lowest energy contour in this third well is 1.5 kcal mol^{-1} higher than the global

Table V. ϕ, ψ Angles for Representative Conformations Extracted from the Calculated Local Energy Minima[a] and the Average ϕ, ψ Angles Computed from the NMR-Derived DG/SA Structures[b]

structure	ϕ_1	ψ_1	ϕ_2	ψ_2	energy (kcal mol^{-1})	population of local energy minimum, %
IB (calculated) (1)	53.9	−149.8	−54.0	−39.8	2.52	100
IA (NMR average)	97.0 ± 23.7	−143.9 ± 10.9	−72.0 ± 4.8	−10.0 ± 5.9		
IIB (calculated (1)	71.1	−149.9	−55.2	−39.9	19.5	66
(2)	78.2	−149.9	−39.9	60.0	20.0	29
(3)	128.1	−59.9	−76.2	60.0	21.0	5
IIA (NMR average)	64.4 ± 6.6	−151.5 ± 8.2	−85.9 ± 1.4	−44.3 ± 3.4		
IIIB (calculated) (1)	68.9	−150.1	−58.9	−39.9	9.5	43
(2)	71.2	−159.9	−70.1	60.0	9.0	57
IIIA (NMR average)	57.1 ± 2.4	−144.3 ± 14.4	−84.0 ± 1.7	45.0 ± 5.2		

[a] Only local energy minima found in the lowest 5 kcal mol^{-1} of the overall potential energy surface were considered for the model compounds IB, IIB, and IIIB. [b] The average ϕ, ψ dihedral angle values for residues $i + 1$ and $i + 2$ in peptides IA, IIA, and IIIA were calculated from the 30 DG/SA structures which incorporated NMR-derived distance restraints.

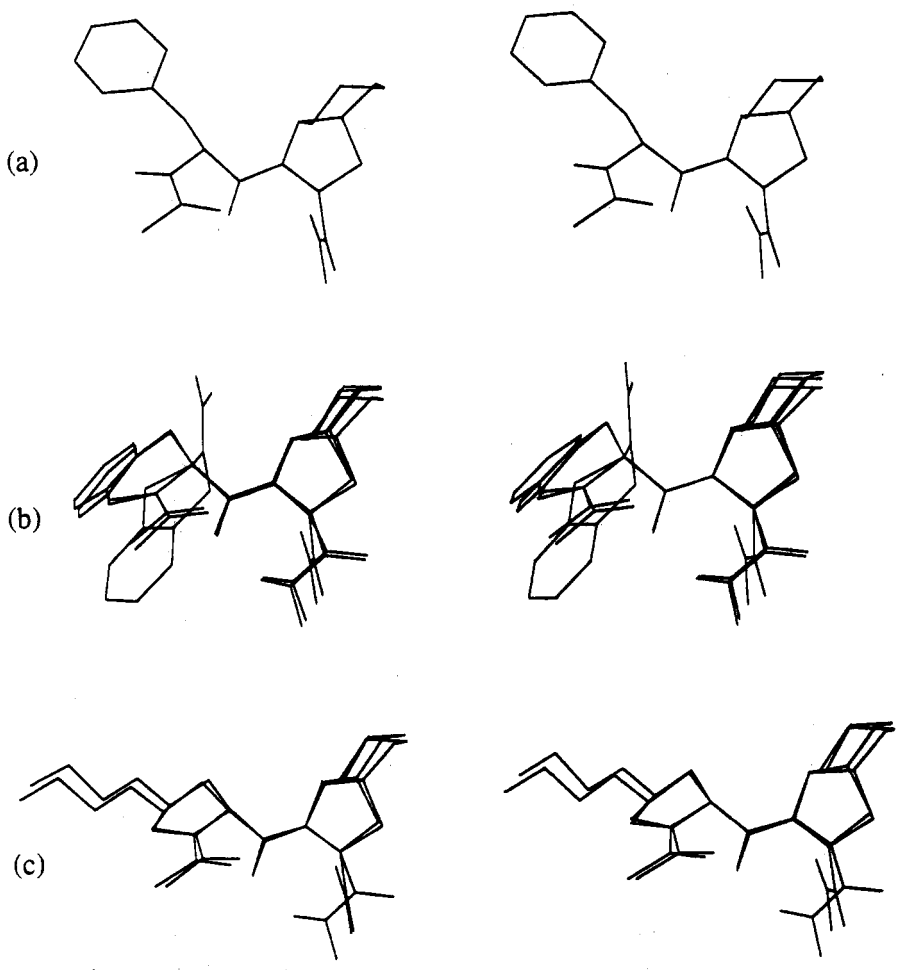

Figure 2. Calculated structures representing each of the local energy minima from the lowest 5 kcal mol^{-1} of the overall potential energy surface for (a) model IB, (b) model IIB, and (c) model IIIB.

minimum. Representative conformations extracted from this well are not β-turn-containing, but instead adopt a twist backbone which incorporates an inverse γ-turn about the Oic residue. On the basis of a Boltzmann population analysis, the relative populations for each potential energy well containing an ensemble of related structures are 66%, 29%, and 5%, respectively. The β-turn-like conformations are expected to be populated to the extent of 95%, overall. The ϕ, ψ values and corresponding energies for representative conformations extracted from each of the three energy wells are tabulated and presented in Table V. Three representative conformations, one from each local energy minimum, are shown together in Figure 2b.

1D. Analysis of Model IIIB. There are two local energy minima of approximately equivalent area in the lowest 5 kcal mol^{-1} of the overall potential energy surface of the two obtained from 10° grid scan about the dihedral angles ψ_1 and ψ_2 in model IIIB. The deepest potential energy well is centered about $\psi_1 = -165.0°$, $\psi_2 = +45.0°$, has a value of 9.0 kcal mol^{-1}, and is separated by a barrier of 1.0 kcal mol^{-1} from the other local energy minimum. Overall, these backbone conformations are very similar to those determined for model IIB; therefore, both are β-turn-like. From Boltzmann calculations, the relative populations are 43% and 57%, respectively. Moreover, with an energy barrier of 1.0 kcal mol^{-1} separating these two related conformers, a rapid rate of conformational interconversion might be anticipated. The ϕ, ψ values and corresponding potential energies for representative conformations extracted from each of the two wells are presented in Table

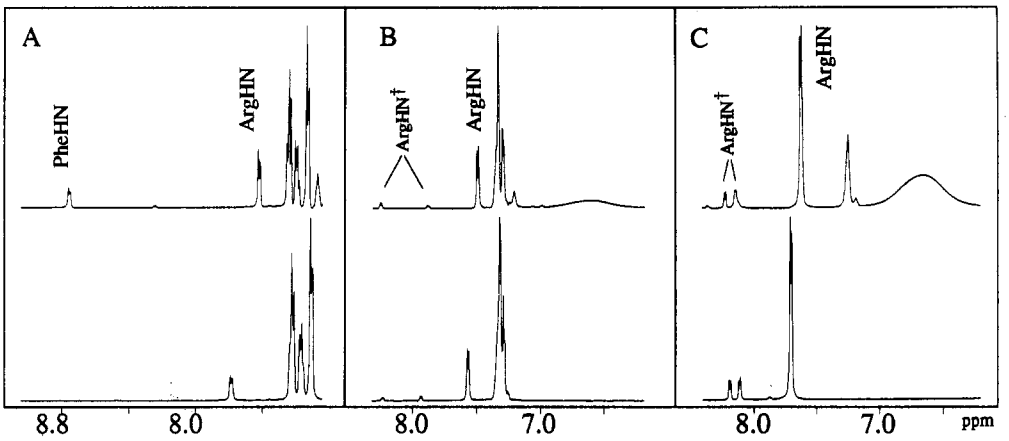

Figure 3. Downfield regions of the ^{1}H NMR spectra of tetrapeptides IA, IIA, and IIIA (spectra A–C, respectively) as a function of pH. All spectra were collected with 2.0 s of Dante solvent presaturation for the suppression of the water resonance. The top spectra were collected at low pH values (~4.4) while the lower spectra were collected at pH values of ~7.7. The relative intensity of the amide signal of Arg^4 in all three tetrapeptides is unaffected by increasing pH values indicating that it is involved in a hydrogen bond. Signals for rapidly exchanging protons (e.g., the amide proton of Phe^2) are unobservable at elevated pH. The weak amide resonances in **B** and **C** that are denoted by daggers are due to minor conformational isomers.

V. Two representative conformations, one from each local energy minimum, are shown together in Figure 2c.

2. NMR Spectra of Bradykinin Antagonist Models. The downfield regions of the ^{1}H NMR spectra of IA–IIIA are shown in Figure 3. As can be seen in this figure, IA exhibits a single set of ^{1}H NMR resonances, whereas IIA and IIIA each exhibit signals for a major species and two minor species. Exchange cross peaks observed in the 2D NOESY data (below) indicate that these species are conformational isomers rather than impurities, and a rate analysis indicates that these conformational isomers undergo interconversion at a rate that is "moderately-slow" (k_{exch} ca. 10 s^{-1} at 37.5 °C) on the NMR time scale.

Figure 3 also shows the important pH behavior of the exchangeable amide protons of peptides IA–IIIA. ^{1}H NMR data obtained at low pH (4.4) and high pH (7.7) are shown at the top and bottom of Figure 3, respectively. For IA, the backbone amide proton of Phe^2 is observable at low pH, where exchange with water protons is relatively slow. However, at neutral pH, this signal is not observed due to rapid chemical exchange with the presaturated water protons. This behavior is typical of solvent-accessible amide protons that do not participate in significant intrapeptide hydrogen bonding. In contrast, the backbone amide proton of Arg^4 is virtually unaffected by the increase in pH, and this reduced exchange rate indicates that the Arg^4 amide proton is involved in internal hydrogen bonding. For large, globular proteins, reduced amide proton exchange rates are also observable for protons that are effectively sequestered from solvent in the hydrophobic core. However, this explanation for the reduced exchange rate of the Arg^4 backbone amide proton of tetrapeptide IA seems implausible. Essentially identical results were obtained for peptides IIA and IIIA, where the amide protons of Arg^4 were the only exchangeable protons observed to be insensitive to solvent presaturation at neutral pH.

^{1}H NMR signals for the major isomers of IA–IIIA were assigned from the two-dimensional homonuclear-correlated NOESY, HOHAHA, and DQF-COSY spectra and the heteronuclear-correlated ^{1}H–^{13}C HMQC spectra following standard procedures. Portions of the 2D NOESY spectrum obtained for IIIA are shown in Figure 4, and examples of the 2D HOHAHA, COSY, and ^{1}H–^{13}C HMQC spectra obtained for IIIA are provided in the supplementary materials (Figures S1–S3, respectively). As can be seen in Figure 4, an antiphase relationship exists between the auto and cross peaks, and this reflects the positive Overhauser effect expected for this small, rapidly tumbling molecule.

^{1}H and ^{13}C NMR signal assignments were made following a standard protocol, whereby proton scalar spins systems are identified in the HOHAHA spectrum (Figure S1), and direct scalar interproton connectivities are determined from the COSY spectrum (Figure S2). Chemical shift degeneracies precluded the assignment of the Oic protons on the basis of the homonuclear correlated spectra alone, however, by correlating protons with their attached ^{13}C resonances, these degeneracies could be easily overcome (Figure S3). This method is particularly useful for assigning geminal protons since they correlate with a single carbon frequency. ^{1}H NMR signal assignments for IA and for the major isomers of IIA and IIIA are listed in Table VI. Unfortunately, efforts to unambiguously assign the ^{1}H NMR signals of the minor isomers were unsuccessful due to (i) the low signal intensities for the minor isomers, which represent no more than 10% concentration relative to the major isomer, (ii) the high amount of chemical shift degeneracy, and (iii) the relatively weak NOE cross peak intensities obtained for these rapidly-tumbling, small molecules with $\omega\tau_c$ values approaching 1.12.

Subsequent to ^{1}H NMR signal assignment, the 2D NOESY data obtained for IA–IIIA were analyzed in order to identify proton pairs with internuclear separations less than ca. 4.5 Å. Intense cross peaks denoted by circles (Figure 4) provide conformational information essential for structural modeling. For example, interresidual cross peaks are observed for the amide proton of Arg^4 to Oic-Hϵ2s and D-Hype(*trans*-propyl)-Hα, D-Hype(*trans*-propyl)-Hα to Oic-Hδ, and Oic-Hδ to D-Hype(*trans*-propyl)-Hβr,s proton pairs. In addition, intraresidue NOEs involving the OicHδ and OicHζ2r proton pair were observed, which enabled identification of the conformation of the Oic 6-membered ring.

The downfield portion of the 2D NOESY spectrum of IIIA is shown in the left portion of Figure 4. This portion of the spectrum is plotted at a 3-fold lower intensity relative to the upfield region in order to show the Arg^4 amide proton signals observed for the minor isomers. The amide proton signals from Arg^4 at 7.56 and 8.10 ppm (which arise from the major and one of the minor conformers, respectively) exhibit NOE cross peaks to the D-Hype(*trans*-propyl)-Hα

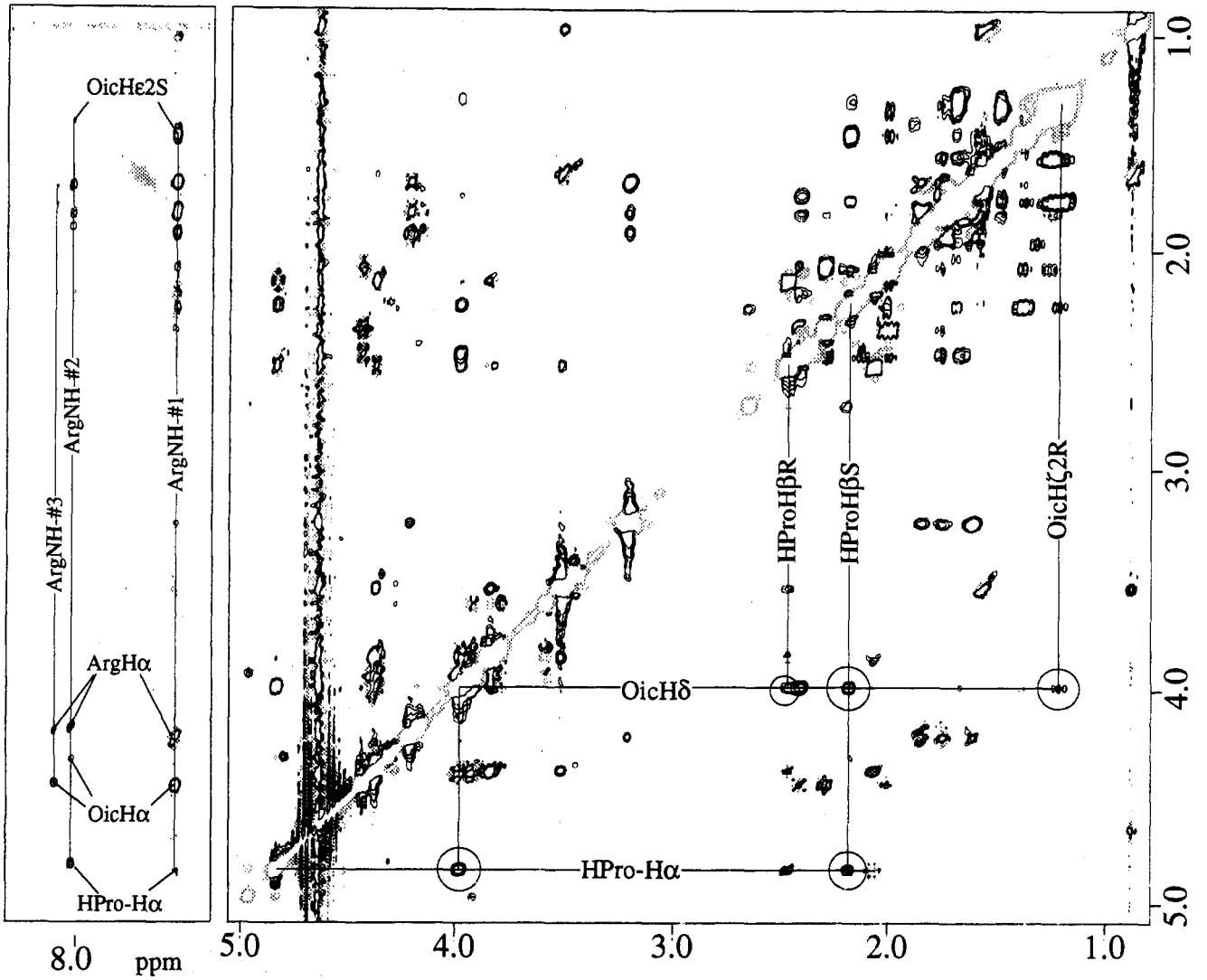

Figure 4. The 500-MHz 2D-NOESY spectrum of tetrapeptide IIIA in 90% H_2O/10% D_2O, pH ~4.4, T = 37.5 °C. Circled NOE cross peaks define the turn structure conformation of this tetrapeptide in solution. The fingerprint region of the spectrum (left) is displayed at a ~3-fold lower counter level to allow cross peaks arising for the minor conformers to be observed.

and Oic-Hε2s protons. As discussed below, the presence of these NOE cross peaks provides strong evidence that the Arg[4] amide proton is oriented in a manner consistent with the calculated turn conformation described in previous sections. The intensity of the third isomer was not sufficient to allow observation of similar NOE signals, and it is possible that this isomer does not adopt the desired turn.

3. NMR-Derived Bradykinin Antagonist Models. Stereo figures showing the simulated annealing/distance geometry (SA/DG) structures for all three tetrapeptides are shown in Figures 5–7. Structures generated with only primary distance restraints exhibit substantial scatter and do not converge to a unique conformation (top stereo pair of Figures 5–7), indicating that the primary restraints by themselves are insufficient to define a unique conformation and that the small molecule modeling parameters are appropriate.[35] In contrast, the backbone atoms of Ser[1]-(O) through Arg[4](N) for structures generated with inclusion of the NMR-derived distance restraints converged to a unique conformation, with the Ser[1] carbonyl and the Arg[4] amide atoms oriented in a manner consistent with tight-turn hydrogen bonding (Figures 5–7, middle and bottom). Table VII lists the standard deviation values obtained upon superposition of the backbone C, Cα, N atoms of residues 2 and 3 for the structures generated with and without NMR restraints. Significantly larger standard deviation values are obtained for the carbonyl of residue 1 and the amide of residue 4 for structures generated without NOE distance restraints (1.9–2.3 Å) compared to those generated with NOE restraints (0.1–0.9 Å), which is also reflected by the scatter of these atoms in Figures 5–7. The average ϕ and ψ values exhibited by the NOE-refined DG/SA structures (Table V) are consistent with the presence of a β-turn in all three tetrapeptides. In addition, for peptides IIA and IIIA, average ϕ and ψ values also indicate the presence of a γ-turn within the β-turn that is defined by a hydrogen bond between the backbone oxygen atom of residue 2 and the backbone amide proton of Arg[4]. The backbone conformations of the DG/SA models are fully consistent with the conformations predicted from systematic searches performed via empirical energy calculations as reflected by the excellent agreement in observed and calculated ψ_1 and ψ_2 values (Figure 1).

Although the DG/SA models of all three tetrapeptides contain a β-turn, the degree of convergence is not identical. Thus, for IA, the standard deviations in backbone atom positions are generally larger than observed for IIA and IIIA, and this is also reflected by the increased scatter in the stereo drawings (Figures 5–7). The scatter observed for the amide proton of Arg[4] is likely due to the lack of

Table VI. ^{1}H Chemical Shift Assignments for Peptides IA–IIIA, pH ~4.5, T = 37.5 °C

residue	chemical shift δ (ppm)[a] HN	Hα	Hβ	others
IA				
Ser [1]		4.11	3.86, 3.93	
D-Phe [2]	8.8	4.94	3.01, 3.08	aromatics 7.28
Oic [3]		4.22	1.78, 2.07	Hγ 1.45; Hδ 3.26 Hε1,1′ 1.06, 1.59 Hε2,2′ 1.23, 1.83 Hζ1,1′ 1.14, 1.33 Hζ2,2′ 1.03, 1.34
Arg [4]	7.59	4.18	1.72, 1.84	γCH$_2$ 1.57, 1.57 δCH$_2$ 3.19, 3.19 HN 7.22
IIA				
Ser [1]		4.71	3.81, 3.88	
D-Tic [2]		5.01	3.04, 3.34	Hε1,1′ 4.81, 4.81 aromatics 7.34
Oic [3]		4.37	1.99, 2.30	Hγ 2.50; Hδ 4.12 Hε1,1′ 1.26, 1.78 Hε2,2′ 1.40, 2.27 Hζ1,1′ 1.30, 1.51 Hζ2,2′ 1.21, 1.72
Arg [4]	7.45	4.22	1.74, 1.83	γCH$_2$ 1.58, 1.58 δCH$_2$ 3.19, 3.19 HN 7.19
IIIA				
Ser [1]		4.41	3.95, 4.01	
D-Hype(*trans*-propyl) [2]		4.86	2.09, 2.49	Hγ 4.39 δCH$_2$ 3.85, 3.85 εCH$_2$ 3.53, 3.53 φCH$_2$ 1.59, 1.59 ζCH$_3$ 0.90
Oic [3]		4.46	2.03, 2.32	Hγ 2.43; Hδ 4.00 Hε1,1′ 1.71, 1.77 Hε2,2′ 1.40, 2.20 Hζ1,1′ 1.28, 1.49 Hζ2,2′ 1.24, 1.51
Arg [4]	7.56	4.22	1.77, 1.87	γCH$_2$ 1.63, 1.63 δCH$_2$ 3.23, 3.23 HN 7.22

[a] Chemical shifts were referenced to H_2O, 4.653 ppm at 37.5 °C.

an observable Arg^{4}HN-to-Phe^{2}Hα cross peak in the NOESY spectrum of peptide IA. An associated distance restraint, which was included to generate structures of IIA and IIIA due to the observation of weak Arg^{4}HN-to-Phe^{2}Hα cross peaks, could not be used to generate the IA models. It is possible that this cross peak was not observed for IA because the Hα proton NMR signal of Phe^2 is situated near the presaturated H_2O solvent signal in the NMR spectrum. The higher degree of scatter observed for the Ser^1 carbonyl of peptide IA is likely due to its higher intrinsic conformational freedom, since the dihedral angle ϕ in Phe^2 is not constrained. The dihedral angle ϕ in residue 2 is constrained in IIA and IIIA since it is incorporated into 6- and 5-membered rings, respectively. The degree of convergence of the remaining two peptides (IIA, IIIA) is almost identical, Table VII.

Substantial effort was made to determine the structural properties of the minor isomers. Unfortunately, due to the high degree of signal degeneracy and the weak nuclear Overhauser effects (due to the fact that $\omega\tau_c \approx 1$ for these small molecules), detailed structure calculations were not feasible. However, some insights into the structural nature of these minor isomers could be gained from qualitative analysis of the NMR data. Thus, the exchange rates of the Arg^4 amide proton in all major and minor isomers were insensitive to pH, suggesting that these protons are all involved in hydrogen bonding. Interestingly, the chemical shifts of the Arg^4 amide proton in the minor isomers are at lower field compared to the major isomers (ca. 0.5 ppm), indicating some local structural change. A few signals for the Oic 6-membered ring were also shifted. In some cases (i.e. for the minor isomers of IIIA), the Arg^4 amide proton to the D-Hype(*trans*-propyl)^2-Cα proton and Arg^4 amide proton to Oic-Hε2s NOE cross peaks were sufficiently strong to add further support for the turn structures (Figure 4). Thus, qualitative interpretation of the limited chemical shift and NOE data for the minor isomers suggests that the structural differences are related to differential puckering of the 6-membered Oic ring, with possible concomitant (minor) reorientation of the Arg-NH bond.

Conclusions

Structural studies have been carried out on tetrapeptides corresponding to the four C-terminal amino acid residues of three highly potent bradykinin receptor antagonists. NMR-derived models for each tetrapeptide exhibit β-turns that are consistent with the conformations predicted by empirical calculations. The high degree of correlation between the calculated and experimentally-derived models is illustrated in Figure 1. It is significant that the models generated using a standard NMR-based DG/SA modeling approach, which does not explicitly account for nonbonded interactions, leads to structures that are essentially identical to those predicted in the absence of experimental data from empirical calculations.

These studies provide the first evidence that second-generation bradykinin antagonists contain C-terminal β-turn conformations. Although studies were performed on C-terminal fragments of the decapeptides, the combined results from computational simulations and NMR experiments make it highly probable that similar turn structures will exist in the full length antagonists. The high affinities of the parent decapeptides, considered together with the high propensity for induction of β-turn conformations about D-Phe-Oic, D-Tic-Oic, and D-Hype(*trans*-propyl)-Oic, as reported in this paper, strongly support the hypothesis that high-affinity peptide bradykinin receptor antagonists adopt C-terminal β-turn conformations when bound to receptor.

Our combined methodologies of NMR and computational chemistry led to the same overall results, making this work an example of the synergy within these two disciplines. The results presented in this paper lend support to the hypothesis that contributing to the functional difference between bradykinin receptor agonists and antagonists is the type of β-turn adopted at the C-terminal end of the ligands, since bradykinin has also been shown to adopt a C-terminal β-turn in several different solvent environments.[21,22]

Experimental Section

H-Ser-D-Tic-Oic-Arg-OH. One gram of Boc-Arg-PAM resin (0.6 mmol/g, 0.6 mmol), Boc-D-Tic, Boc-Oic, and Boc-Ser(O-Bz) were loaded in the synthesizer according to the sequence starting from the C-terminus. The resin was washed twice with methylene chloride (wash A) and three times with 1:1 dimethylformamide/methylene chloride (wash B) at the beginning of the synthesis and after each step. Each wash was for 40 s. The removal of the BOC protection was performed using a deblocking solution (15 mL), containing 45% trifluoroacetic acid, 50% methylene chloride, and 5% anisole. Subsequently, the resin was washed three times each with washes A and B, followed by three washes with base (15 mL) containing 10% *N,N′*-diisopropylethylamine in methylene chloride. This was followed by two washes with A and three washes with B. The coupling step was performed using

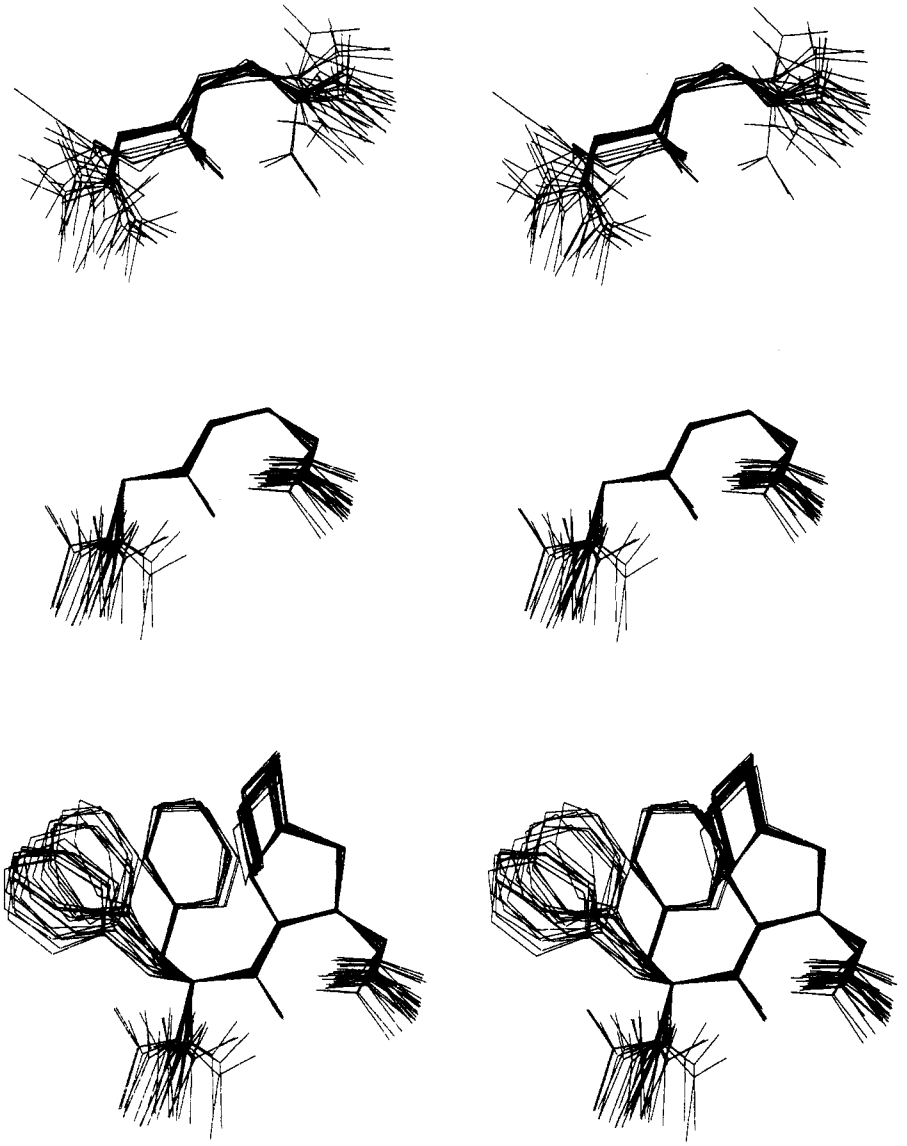

Figure 5. Stereoviews showing the best-fit superpositions of the C, Cα, and N atoms of residues 2 and 3 of tetrapeptide IA. The top stereoview depicts the 30 DG/SA structures generated with only primary distance restraints, while the middle and lower images depict the 30 DG/SA structures generated with the addition of NOE restraints. Atoms displayed in all stereoviews include Cα, C, and O (1); C, Cα, N, O (2); C, Cα, N (3); Cα, N, HN (4); the bottom stereo pair also includes all heavy atoms of residues 2 and 3.

a 3-fold excess (1.8 mmol) of the protected amino acid, in dimethylformamide, simultaneously mixed with an equivalent quantity of activator solution containing 1,3-diisopropylcarbodiimide in methylene chloride. All amino acids were coupled according to the sequence starting from the C-terminus, for 2 h and two times each. The peptide resin was dried, weighed, and transferred to a Teflon tube containing a magnetic stirring bar and was treated with anisole, 100 mL/g resin. Hydrogen fluoride was condensed using a dry ice/acetone bath, from a tank attached to hydrogen fluoride cleavage apparatus (Immunodynamics, La Jolla, CA). After the condensation, the dry ice/acetone bath was replaced with an ice water bath, and the reaction mixture was stirred for 1 h. The hydrogen fluoride was then removed using a stream of nitrogen through a KOH trap. The peptide resin was further dried using aspirator and high vacuum. Subsequently it was washed with ether (3 × 20 mL/g resin) and extracted with 0.1% TFA (3 × 20 mL/g resin). The solution of the peptide was frozen and lyophilized. The crude product was purified using reverse-phase HPLC on a C_{18} Vydac column (22.5 × 250 cm, 300-Å pore size). The solvent system was 0.1% TFA in water/acetonitrile (0.1% TFA), and the gradient was 5–40% acetonitrile over 30 min. Each fraction was analyzed by analytical reverse-phase HPLC, and the clean fractions were combined and lyophilized to give a homogeneous white powder. The purity of the final product was confirmed by analytical HPLC, FABMS, and amino acid analysis.

H-Ser-D-Phe-Oic-Arg-OH. One gram of Boc-Arg-PAM resin (0.6 mmol/g, 0.6 mmol), Boc-D-Phe, Boc-Oic, and Boc-Ser(O-Bz) were loaded in the synthesizer according to the sequence starting from the C-terminus. The resin was washed twice with methylene chloride (wash A) and three times with 1:1 dimethylformamide/methylene chloride (wash B) at the beginning of the synthesis and after each step. Each wash was for 40 s. The removal of the BOC protection was performed using a deblocking solution (15 mL), containing 45% trifluoroacetic acid, 50% methylene chloride, and 5% anisole. Subsequently, the resin was washed three times each with washes A and B, followed by three washes with base (15 mL) containing 10% *N,N'*-diisopropylethylamine in methylene chloride. This was followed by two washes with A and three washes with B. The coupling step was performed using a 3-fold excess (1.8 mmol) of the protected amino acid, in dimethylformamide, simultaneously mixed with an equivalent quantity of activator solution containing 1,3-diisopropylcarbodiimide in methylene chloride. All amino acids were coupled according to the sequence for 2 h and two times each starting from the C-terminus. The peptide resin was dried, weighed, and transferred to a Teflon tube, containing a magnetic stirring bar and treated with anisole, 100 mL/g resin. Hydrogen fluoride was condensed using a dry ice/acetone bath from a tank attached to a hydrogen fluoride cleavage apparatus (Immunodynamics, La Jolla, CA). Following the condensation, the dry ice/acetone bath was replaced with an ice bath, and the reaction mixture was

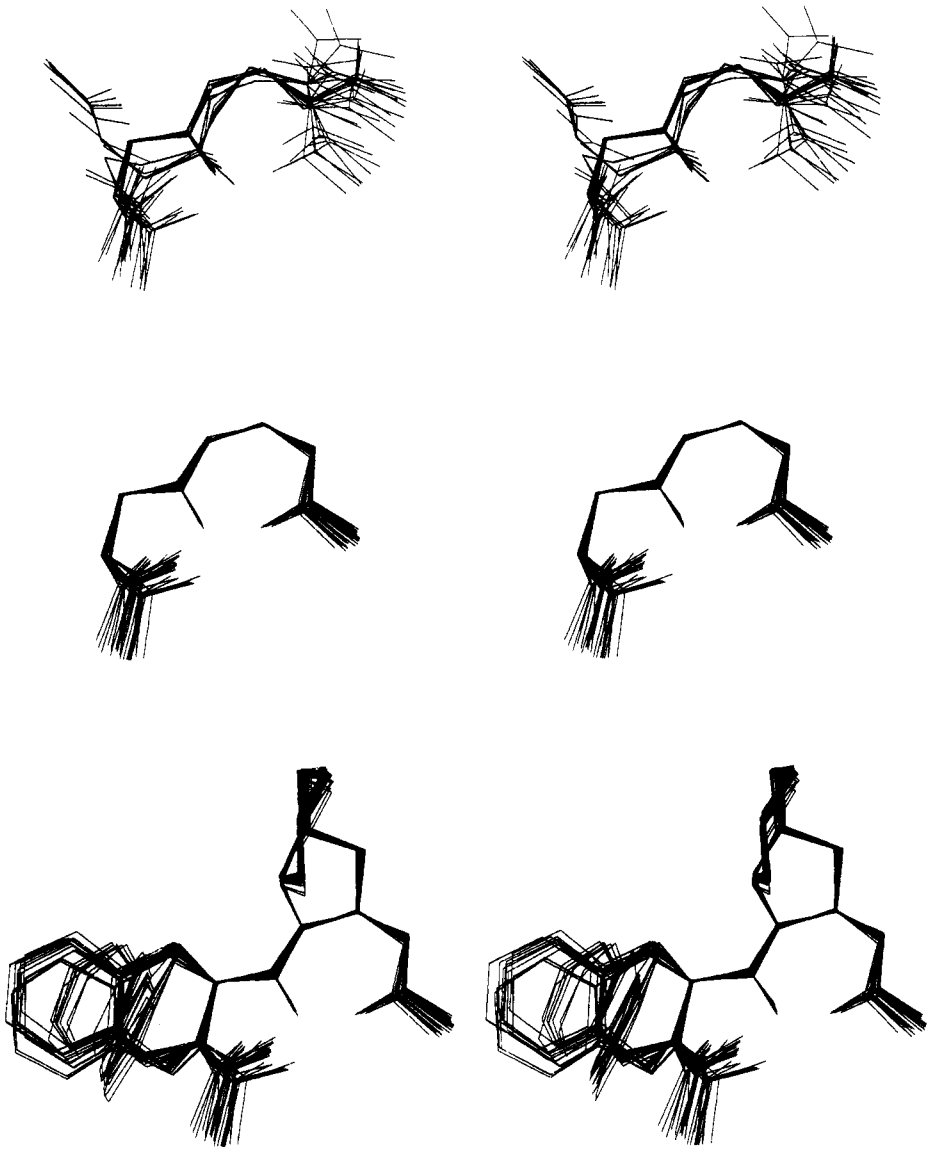

Figure 6. Stereoviews showing the best-fit superpositions of the C, Cα, and N atoms of residues 2 and 3 of tetrapeptide IIA. The top stereoview depicts the 30 DG/SA structures generated with only primary distance restraints, while the middle and lower images depict the 30 DG/SA structures generated with the addition of NOE restraints. Atoms displayed in all stereoviews include Cα, C, and O (1); C, Cα, N, O (2); C, Cα, N (3); Cα, N, HN (4); the bottom stereo pair also includes all heavy atoms of residues 2 and 3.

stirred for 1 h. The hydrogen fluoride was then removed using a stream of nitrogen through a KOH trap. The peptide resin was further dried using an aspirator and high vacuum. Subsequently it was washed with ether (3 × 20 mL/g resin) and extracted with 0.1% TFA (3 × 20 mL/g resin). The solution of the peptide was frozen and lyophilized. The crude product was purified using reverse-phase HPLC on a C_{18} Vydac column, (22.5 × 250 cm, 300-Å pore size). The solvent system was 0.1% TFA in water/acetonitrile (0.1% TFA), and the gradient was 5–40% acetonitrile over 30 min. Each fraction was analyzed by analytical reverse-phase HPLC, and the clean fractions were combined and lyophilized to give a homogeneous white powder. The purity of the final products were confirmed by analytical HPLC, FABMS, and amino acid analysis.

H-Ser-D-Hype(*trans*-propyl)-Oic-Arg-OH. One gram of Boc-Arg-PAM resin (0.6 mmol/g, 0.6 mmol), Boc-D-Hype(*trans*-propyl), Boc-Oic, and Boc-Ser(O-Bz) were loaded in the synthesizer according to the sequence starting from the C-terminus. The resin was washed twice with methylene chloride (wash A) and three times with 1:1 dimethylformamide/methylene chloride (wash B) at the beginning of the synthesis and after each step. Each wash was for 40 s. The removal of the BOC protection was performed using a deblocking solution (15 mL), containing 45% trifluoroacetic acid, 50% methylene chloride, and 5% anisole. Subsequently, the resin was washed three times each with washes A and B, followed by three washes with base (15 mL) containing 10% *N,N'*-diisopropylethylamine in methylene chloride. This was followed by two washes with A and three washes with B. The coupling step was performed using a 3-fold excess (1.8 mmol) of the protected amino acid, in dimethylformamide, simultaneously mixed with an equivalent quantity of activator solution containing 1,3-diisopropylcarbodiimide in methylene chloride. All amino acids were coupled for 2 h and two times each according to the sequence. The peptide resin was dried, weighed, and transferred to a Teflon tube, containing a magnetic stirring bar and treated with anisole, 100 mL/g resin. Hydrogen fluoride was condensed using a dry ice/acetone bath, from a tank attached to hydrogen fluoride cleavage apparatus (Immunodynamics, La Jolla, CA). Following the condensation, the dry ice/acetone bath was replaced with an ice water bath, and the reaction mixture was stirred for 1 h. The hydrogen fluoride was then removed using a stream of nitrogen through a KOH trap. The peptide resin was further dried using aspirator and high vacuum. Subsequently, it was washed with ether (3 × 20 mL/g resin) and extracted with 0.1% TFA (3 × 20 mL/g resin). The solution of the peptide was frozen and lyophilized. The crude product was purified using reverse-phase HPLC on a C_{18} Vydac column (22.5 × 250 cm, 300-Å pore size). The solvent system was 0.1% TFA in water/acetonitrile (0.1% TFA), and the gradient was 5–40% acetonitrile over 30 min. Each fraction was analyzed by analytical reverse-phase HPLC, and the clean fractions were combined and lyophilized to give a homogeneous white fluffy powder. The purity of the final products were confirmed by analytical HPLC, FABMS, and amino acid analysis.

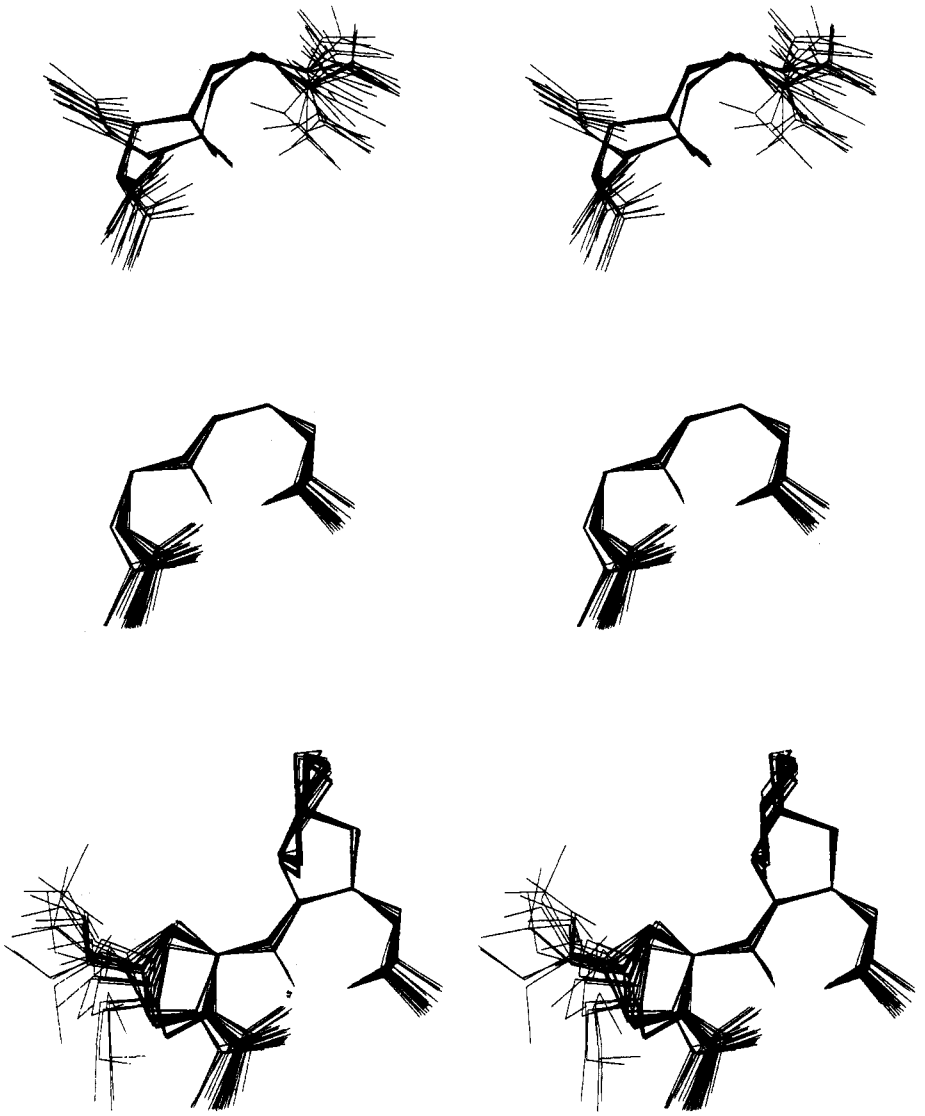

Figure 7. Stereoviews showing the best-fit superpositions of the C, Cα, and N atoms of residues 2 and 3 of tetrapeptide IIIA. The top stereoview depicts the 30 DG/SA structures generated with only primary distance restraints, while the middle and lower images depict the 30 DG/SA structures generated with the addition of NOE restraints. Atoms displayed in all stereoviews include Cα, C, and O (1); C, Cα, N, O (2); C, Cα, N (3); Cα, N, HN (4); the bottom stereo pair also includes all heavy atoms of residues 2 and 3, with the exception of the terminal methyl of the trans propyl ether.

Table VII. Standard Deviation (Å) for Specific Atoms in DG/SA Structures[a]

	primary restraints[b]			NMR restraints[c]		
peptide	O[1]	O[2]	HN[4]	O[1]	O[2]	HN[3]
IA	2.25	0.71	1.87	0.92	0.19	0.29
IIA	2.27	0.48	1.96	0.60	0.12	0.15
IIIA	2.34	0.31	2.00	0.49	0.18	0.25

[a] Standard deviations were calculated for each set of 30 DG/SA structures following superposition of C, Cα, and N atoms of residues 2 and 3. The lowest penalty structure was kept stationary. [b] DG/SA structures generated with only the primary sequence information (e.g., bond lengths, angles, atomic radii). [c] DG/SA structures generated will loose restraints obtained from NOESY data.

N-Boc-D-*trans*-4-*n*-propoxyproline. To a stirred suspension of sodium hydride (2.04 g, 80%, 68.0 mmol) [washed with anhydrous hexane (2 × 15 mL)] in anhydrous dimethylformamide (60 mL) was added a solution of N-Boc-D-*trans*-4-hydroxyproline (6.05 g, 26.1 mmol) in anhydrous dimethylformamide (30 mL) at room temperature under argon. After 30 min, the mixture was treated with allyl bromide (5.66 mL, 65.4 mmol). After 21 h, the reaction mixture was diluted with water (50 mL) and the mixture acidified with aqueous hydrochloric acid (5 N) to the Congo Red indicator endpoint. The mixture was extracted with diethyl ether (3 × 130 mL), and the combined extracts were dried over sodium sulfate and concentrated to an oil which was used directly in the next step without purification. To a stirred solution of the crude product in methanol (30 mL) was added a solution of aqueous sodium hydroxide (25 mL, 3 N, 75 mmol) at room temperature. After 18 h, water (20 mL) was added followed by aqueous hydrochloric acid (5 N) to adjust the pH of the solution to 10, and then the solution was extracted with diethyl ether (2 × 25 mL). The combined organic layers were discarded. The aqueous layer was further acidified to the Congo Red indicator endpoint and extracted with ethyl acetate (3 × 100 mL). The combined ethyl acetate extracts were dried over sodium sulfate and concentrated to an oil. A suspension of the above product and 5% palladium on activated carbon (0.37 g) in ethyl acetate (80 mL) was shaked under 30 psi of hydrogen at room temperature. After 17 h, the catalyst was removed and washed with ethyl acetate. The combined filtrates were concentrated in an oil. Flash chromatography (silica gel, 25% methanol in dichloromethane) gave the desired product (4.36 g, overall yield 64.8%) as an oil: IR (neat film, cm^{-1}) 3550–2550 (broad), 2974, 2936, 2879, 1750, 1704, 1399, 1367, 1162, 1097, 1010, 907, 856, 771; ^1H NMR (300 MHz, $CDCl_3$) ppm 0.91 (t, 3 H, J = 7.2 Hz), 1.43 and 1.48 (2 s, 9 H), 1.57 (q, 2 H, J = 7.2 Hz), 2.24 (m, 2 H), 3.37 (m, 2 H), 4.05 (m, 1 H), 4.40 (m, 1 H), 9.92 (s, 1 H). Dicyclohexylamine salt (recrystallized from heptane): mp 118–120 °C; $[\alpha]^{23.5}_D$ = +27.1 (c = 1.03, methanol). Anal. Calcd for $C_{25}H_{46}N_2O_5$ (454.65 g/mol) C, 66.05; H, 10.20; N, 6.16. Found: C, 65.91; H, 10.23; N, 6.19.

Acknowledgment. This work was supported by a grant from the Maryland Industrial Partnership program, MIPS # 1026.10. The 600-MHz NMR instrument was purchased with support of the NIH (GM42561, AI30917).

Supplementary Material Available: 2D HOHAHA, COSY, and ^{1}H–^{13}C HMQC spectra obtained for IIIA (3 pages). Ordering information is given on any current masthead page.

References

(1) Clark, W. G. Kinins and peripheral and central nervous system. In *Bradykinin, Kallidin and Kallikrein. Handbook of Experimental Pharmacology, Vol. XXV*; Erdos, E. G., Ed.; Springer-Verlag: New York, 1979; pp 311–356.

(2) Griesbacher, T.; Lembeck, F. Effect of bradykinin antagonists on bradykinin-induced plasma extravasation, venoconstriction, prostaglandin E_2 release, and nociceptor stimulation and contraction of the iris sphincter muscle in the rabbit. *Br. J. Pharmacol.* **1987**, *92*, 333–340.

(3) Taiwo, Y. O.; Levine, J. D. Characterization of the arachidonic acid metabolites mediating bradykinin and noradrenaline hyperalgesia. *Brain Res.* **1988**, *458*, 402–406.

(4) Steranka, L. R.; Manning, D. C.; DeHaas, C. J.; Ferkany, J. W.; Borosky, S. A.; Connor, J. R.; Vavrek, R. J.; Stewart, J. M.; Snyder, S. H. Bradykinin as a pain mediator: Receptors are localized to sensory neurons, and antagonists have analgesic actions. *Proc. Natl. Acad. Sci. U.S.A.* **1988**, *85*, 3245–3249.

(5) Dray, A.; Bettaney, J.; Forster, P.; Perkins, M. N. Bradykinin-induced stimulation of afferent fibers is mediated through protein kinase C. *Neurosci. Lett.* **1988**, *91*, 301–307.

(6) Steranka, L. R.; Farmer, S. G.; Burch, R. M. Antagonists of B2 bradykinin receptors. *FASEB J.* **1989**, *3*, 2019–2025.

(7) Haley, J. E.; Dickenson, A. H.; Schachter, M. Electrophysiological evidence for a role of bradykinin in chemical nociception in the rat. *Neurosci. Lett.* **1989**, *97*, 198–202.

(8) Marceau, F.; Lussier, A.; Regoli, D.; Giroud, J. P. Pharmacology of kinins: Their relevance to tissue injury and inflammation. *Gen. Pharmacol.* **1983**, *14*, 209–229.

(9) Proud, D.; Kaplan, A. P. Kinin formation: Mechanisms and role in inflammatory disorders. *Annu. Rev. Immunol.* **1988**, *6*, 49–84.

(10) Colman, R. W.; Wong, P. Y. Kallikrein-kinin system in pathologic conditions. In *Bradykinin, Kallidin and Kallikrein. Handbook of Experimental Pharmacology, Vol. XXV*; Erdos, E. G., Ed.; Springer-Verlag: New York, 1979; pp 569–607.

(11) Greaves, M. W. Inflammation and mediators. *Br. J. Dermatol.* **1988**, *119*, 419–426.

(12) Kinins and their Antagonists. *Lancet* **1991**, *338*, 287–288.

(13) Noronha-Blob, L.; Otterbein, L.; Lowe, V. C.; Kyle, D. J.; Hiner, R. N.; Burch, R. M. A bradykinin receptor antagonist reduces mortality in gram negative sepsis in rats. *Br. J. Pharmacol.* In press.

(14) (a) Hock, F. J.; Wirth, K.; Albus, U.; Linz, W.; Gerhards, H. J.; Wiemer, G.; Henke, St.; Breipohl, G.; Knoig, W.; Knolle, J.; Scholkens, B. A. HOE 140 a new potent and long acting bradykinin antagonist: in vitro studies. *Br. J. Pharmacol.* **1991**, *102*, 769–773. (b) Wirth, K.; Hock, F. J.; Albus, U.; Linz, W.; Alpermann, H. G.; Anagnostopoulos, H.; Henke, St.; Breipohl, G.; Knoig, W.; Knolle, J.; Scholkens, B. A. HOE 140 a new potent and long acting bradykinin antagonist: in vivo studies. *Br. J. Pharmacol.* **1991**, *102*, 774–777.

(15) Kyle, D. J.; Martin, J. A.; Farmer, S. G.; Burch, R. M. Design and conformational analysis of several highly potent bradykinin receptor antagonists. *J. Med. Chem.* **1991**, *34*, 1230–1233.

(16) Kyle, D. J.; Martin, J. A.; Burch, R. M.; Carter, J. P.; Lu, S.; Meeker, S.; Prosser, J. C.; Sullivan, J. P.; Togo, J.; Noronha-Blob, L.; Sinsko, J. A.; Walters, R. F.; Whaley, L. W.; Hiner, R. N. Probing the bradykinin receptor: Mapping the geometric topography using ethers of hydroxyproline in novel peptides. *J. Med. Chem.* **1991**, *34*, 2649–2653.

(17) Farmer, S. G.; Burch, R. M.; Kyle, D. J.; Martin, J. A.; Meeker, S. N.; Togo, J. D-Arg[Hyp^{3}-Thi^{5}-D-Tic^{7}-Tic^{8}]-bradykinin, a potent antagonist of smooth muscle BK_2 receptors and BK_3 receptors. *Br. J. Pharmacol.* **1991**, *102*, 785–787.

(18) Stewart, J. M.; Vavrek, R. J. Chemistry of peptide B2 bradykinin antagonists. In *Bradykinin Antagonists: Basic and Clinical Research*; Burch, R. M., Ed.; Marcel-Dekker: New York, 1990; pp 51–96.

(19) Kyle, D. J.; Green, L. M.; Blake, P. R.; Smithwick, D.; Summers, M. F. A novel beta turn mimetic useful for mapping the unknown topology of peptide receptors. *Peptide Res.* **1992**, *5*, 206–209.

(20) (a) Brooks, B. R.; Bruccoleri, R. E.; Olafson, B. D.; States, D. J.; Swaminathon, S.; Karplus, M. J. CHARMM: A program for macromolecular energy, minimization, and dynamics calculations. *J. Comput. Chem.* **1983**, *4*, 187–217. (b) Polygen Corporation, 200 Fifth Avenue, Waltham, MA 12254.

(21) Kyle, D. J.; Hicks, R. P.; Blake, P. R.; Klimkowski, V. J. Conformational properties of bradykinin and bradykinin antagonists. *Bradykinin Antagonists: Basic and Clinical Research*; Burch, R. M., Ed.; Marcel Dekker: New York, 1990; pp 131–146.

(22) Lee, S. C.; Russell, A. F.; Laidig, W. D. Three dimensional structure of bradykinin in SDS micelles. *Int. J. Peptide Protein Res.* **1990**, *35*, 367–371.

(23) Merrifield, R. B. Solid phase peptide synthesis. I. The synthesis of a tetrapeptide. *J. Am. Chem. Soc.* **1963**, *85*, 2149–2154.

(24) Vincent, M.; Remond, G.; Portevin, B.; Serkiz, B.; Laubie, M. Stereoselective synthesis of a new perhydroindole derivative of chiral iminodiacid, a potent inhibitor of angiotensin converting enzyme. *Tetrahedron Lett.* **1982**, *23*, 1677–1680.

(25) States, D. J.; Haberkorn, R. H.; Ruben, D. J. A two-dimensional nuclear Overhauser experiment with pure absorption phase in four quadrants. *J. Magn. Reson.* **1982**, *48*, 286–292.

(26) Hore, J. P. A new method for water suppression in the proton NMR spectra of aqueous solutions. *J. Magn. Reson.* **1983**, *55*, 283–300.

(27) Brown, S. C.; Weber, P. L.; Mueller, L. Toward complete proton NMR spectra in proteins. *J. Magn. Reson.* **1988**, *71*, 166–169.

(28) Blake, P. R.; Park, J. B.; Bryant, F. O.; Aono, S.; Magnunson, J. K.; Eccleston, E.; Howard, J. B.; Summers, M. F.; Adams, M. W. Determinants of protein hyperthermostability: Purification and amino sequence of rubredoxin from the hyperthermophilic archaebacterium *Pyrococcus furiosus* and secondary structure of the zinc adduct by NMR. *Biochemistry* **1991**, *30*, 10885–10895.

(29) Braunschweiler, L.; Ernst, R. R. Coherence transfer by isotropic mixing: Application to proton correlation spectroscopy. *J. Magn. Reson.* **1983**, *53*, 521–528.

(30) Davis, D. G.; Bax, A. Assignment of complex 1H NMR spectra via two-dimensional homonuclear Hartmann-Hahn spectroscopy. *J. Am. Chem. Soc.* **1985**, *107*, 2820–2821.

(31) Pinantini, U.; Sorensen, O. W.; Ernst, R. R. Multiple quantum filters for elucidating NMR coupling networks. *J. Am. Chem. Soc.* **1982**, *104*, 6800–6801.

(32) Bax, A.; Subramanian, S. Sensitivity-enhanced two-dimensional heteronuclear shift correlation NMR spectroscopy. *J. Magn. Reson.* **1986**, *67*, 565–569.

(33) Jeener, B. H.; Meier, P.; Bachmann, P.; Ernst, R. R. Investigation of exchange processes by two-dimensional NMR spectroscopy. *J. Chem. Phys.* **1979**, *71*, 4546–4553.

(34) Macura, S.; Ernst, R. R. Elucidation of cross relaxation in liquids by two-dimensional NMR spectroscopy. *Mol. Phys.* **1980**, *41*, 95–117.

(35) Won, H.; Olson, K. D.; Hare, D. R.; Wolfe, R. S.; Krathy, C.; Summers, M. F. Structural modelling of small molecules by NMR: Solution-state structure of 12,13-diepimeric coenzyme F430 and comparison with the X-ray structure of pentamethyl ester derivative. *J. Am. Chem. Soc.* **1992**, *114*, 6880–6892.

(36) Bothner-by, A.; Stephens, R. L.; Lee, J. T.; Warren, C. D.; Jeanloz, R. W. Structure determination of a tetrasaccharide: Transient nuclear overhauser effects in the rotating frame. *J. Am. Chem. Soc.* **1984**, *106*, 811–813.

(37) Blake, P. R.; Hare, D. N.; Summers, M. F. Is 2-D NOESY back-calculation necessary for NMR-based structure determination? A systematic study involving a retroviral-type zinc finger peptide. In *Techniques in Protein Chemistry II*; Villanfranca, J., Ed.; Academic Press: New York, 1991; pp 357–370.

(38) Blake, P. R.; Park, J. B.; Hare, D. R.; Adams, M. W. W.; Summers, M. F. Solution-state structure by NMR of zinc-substituted rubredoxin from the marine hyperthermophilic archaebacteriun, Pyrococcus furiosus. *Protein Sci.* **1992**, *1*, 1508–1521.

(39) Farmer, S. G.; Burch, R. M.; Dehaas, C. J.; Togo, J.; Steranka, L. R. [Arg^{1}-D-Phe^{7}]-substituted bradykinin analogues inhibit bradykinin- and vasopressin-induced contractions of uterine smooth muscle. *J. Pharm. Exp. Ther.* **1989**, *248*, 677–681.

(40) Mahan, L. C.; Burch, R. M. Functional expression of B2 bradykinin receptors from balb/c cell mRNA in Xenopus Oocytes. *Mol. Pharmacol.* **1990**, *37*, 785–792.